Effects of inertia on the rheology of a dilute emulsion of drops in shear

Xiaoyi Li and Kausik Sarkar[a]

Department of Mechanical Engineering, University of Delaware, Newark, Delaware 19716

Synopsis

Effects of inertia on the rheology of dilute Newtonian emulsion of drops in shear flow are investigated using direct numerical simulation. The drop shape and flow are computed by solving the Navier-Stokes equation in two phases using Front-tracking method. Effective stress is computed using Batchelor's formulation, where the interfacial stress is obtained from the simulated drop shape and the perturbation stress from the velocity field. At low Reynolds number, the simulation shows good agreement with various analytical results and experimental measurements. At higher inertia deformation is enhanced and the tilt angle of the drop becomes larger than forty-five degree. The inertial morphology directly affects interfacial stresses. The first and the second interfacial normal stress differences are found to change sign due to the change in drop orientation. The interfacial shear stress is enhanced by inertia and decreases with capillary number at lower inertia but increases at higher inertia. The total excess stresses including perturbation stress contribution shows similar patterns. © *2005 The Society of Rheology.*
[DOI: 10.1122/1.2048748]

I. INTRODUCTION

Emulsions of drop play a critical role in numerous chemical and processing industries. The rheological properties of such emulsions are determined by the evolving morphology of drop shapes (Tucker and Moldenaers 2002). For certain polymers, the final solid products are made by locking the structure of droplets formed during processing. Rheological measurement can also offer a means for inferring drop shapes. Extensive theoretical and experimental effort has been devoted to investigate the relationship between macroscopic rheology and microstructural mechanics of emulsions. Taylor (1932, 1934) first investigated deformation of drops in linear flows and its effect on the viscosity of emulsions. Batchelor (1970) derived expressions for the stress of a homogeneous suspension as a function of the instantaneous microstructure; the excess interfacial stress due to presence of drops was expressed in terms of an interface tensor (Mellema and Willemse 1983; Onuki 1987). This tensor was utilized by Doi and Ohta (1990) as a description of interfacial morphology for co-continuous microstructures. Tensor theories for ellipsoidal drop deformation were developed based on the work of Maffetone and Minale (1998) by

---

[a]Author to whom correspondence should be addressed; electronic mail: sarkar@me.udel.edu

Wetzel and Tucker (2001) (See Tucker and Moldenaers 2002 for a review). Almusallam *et al.* (2000) and Jansseune *et al.* (2000, 2001) performed rheological test of Newtonian emulsion in transient and steady shear and matched the experiments with these tensor models. Various improvements of the tensor model were suggested by Jackson and Tuker (2002) and Yu and Bousmina (2003) and shown to compare better with experimental data. Recently, the tensor approach was extended to investigate viscoelastic systems (Yu *et al.* 2004, Minale 2004, and Maffettone and Greco 2004). Effects of interfacial surfactants on emulsion rheology were experimentally studied by Velankar *et al.* (2001, 2004). A numerical investigation along with experimental comparison of drop breakup in steady shear is recently reported by Cristini *et al.* (2003).

There has not been much investigation on finite inertia effects on the fluid mechanics of emulsion, even though many industrial flows are turbulent. Inertia could exert significant influence on emulsion rheology. Theoretically, correction for inertial effects has been made while analyzing rheological data for single phase flow [Böhme and Stenger (1990); Aschoff, and Schümmer (1993)]. Effects of inertia on rigid-particle suspension rheology were also explored. Lin and Schowalter (1970) investigated suspensions of rigid spheres in shear, considering finite but small particle Reynolds number. Numerical study at higher particle Reynolds number was performed by Patankar and Hu (2002). Wylie *et al.* (2003) studied averaged rheological properties of suspensions with high particle inertia and moderate fluid inertia. Compared to rigid particles, drops contribute to an added complexity due to their deformation. It is the aim of this paper to study the effects of inertia on the deformation of contained drops in an emulsion and the resulting steady shear rheology of the emulsion.

Large drop deformation at finite inertia can only be analyzed using numerical simulation. We use a Front-tracking method [Tryggvason *et al.* (2001); Sarkar and Schowalter (2001a, 2001b), Li and Sarkar (2005a)] to compute the fluid velocity and drop shapes. The interfacial stress is calculated based on the exact front geometry [Batchelor (1970); Li and Sarkar (2005b)]. We have recently used the same computational technique to investigate oscillating extensional theology of a dilute emulsion of viscous drops at low Reynolds number [Li and Sarkar (2005b)]. Note that the shape of a drop at finite interfacial tension is not exactly ellipsoidal in linear flows [Wetzel and Tucker (2001)]. Like Boundary-element method [Cristini *et al.* (2002a, 2002b)] Front-tracking method can deal with arbitrary interface motion. It can also handle inertial viscoelastic system [Sarkar and Schowalter (2000)]. Li *et al.* (2000) and Renardy and Cristini (2001) used similar Navier-Stokes Volume-Of-Fluid (VOF) formulation to study effects of inertia on drop deformation in shear, without considering its rheological impact.

In the following, we describe the mathematical formulation of the problem. Numerical implementation by Front-tracking is briefly discussed and the reader is referred to Tryggvason *et al.* (2001) and Sarkar and Schowalter (2001a) for more details. Results on morphology and rheology are presented with varying viscosity ratio, capillary number and drop Reynolds numbers. Comparisons with available experimental and analytical data are provided as well.

II. PROBLEM FORMULATION

A. Navier-Stokes formulation

Consider a simple shear flow of Newtonian emulsion between two infinite plates (Fig. 1). The incompressible flow is governed by the momentum (Navier-Stokes) and mass conservation equation in the entire domain Ω consisting of the continuous phase Ω_c and the suspended drops Ω_d:

$$\frac{\partial(\rho \mathbf{u})}{\partial t} + \nabla \cdot (\rho \mathbf{u}\mathbf{u}) = -\nabla p - \int_{\partial \mathbf{B}} d\mathbf{x_B} \kappa \mathbf{n} \Gamma \, \delta(\mathbf{x} - \mathbf{x_B}) + \nabla \cdot [\mu \{\nabla \mathbf{u} + (\nabla \mathbf{u})^T\}],$$

$$\nabla \cdot \mathbf{u} = 0 \tag{1}$$

where p is the pressure, ρ the density, and μ the viscosity of the fluid. The superscript ^{T} represents transpose. ∂B is the drop interface consisting of points $\mathbf{x_B}$, Γ is the constant interfacial tension, κ the local curvature, $\mathbf{n}$ the outward normal to the interface, and $\delta(\mathbf{x} - \mathbf{x_B})$ is the three-dimensional Dirac delta function. The interfacial tension, which produces a jump in the normal stress across the interface, is represented as a singular
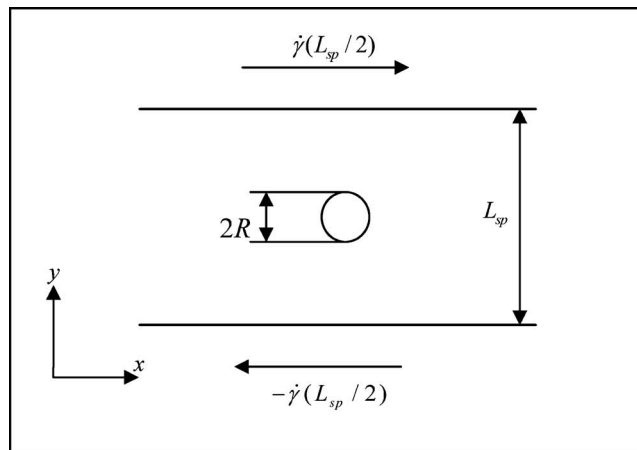
(a)
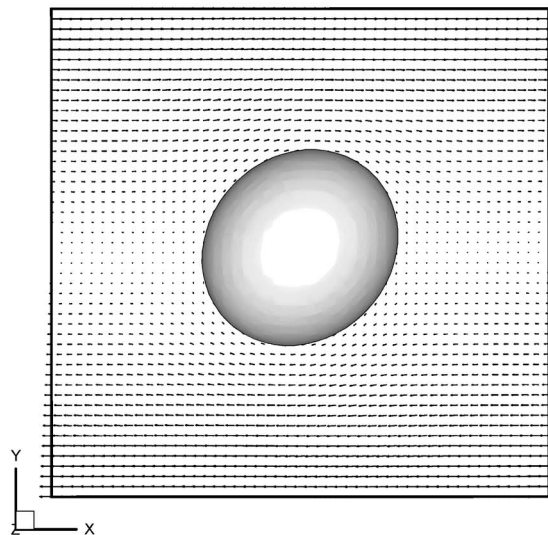
(b)

FIG. 1. (a) Sketch of a drop in a simple shear. $\dot{\gamma}$ is the shear rate, z axis is in the direction orthogonal to the x-y plane. (b) The deformed drop in simple shear at Re=1.0 Ca=0.05. The velocity vectors are in the x-y plane cutting through the center of the drop.

body force (second term on the right). The deformed drop shape generates an anisotropic contribution to the stress field through this term. The interface $\mathbf{x_B}$ is advected by the fluid velocity $\mathbf{u}$:

$$\frac{d\mathbf{x_B}}{dt} = \mathbf{u}(\mathbf{x_B}). \tag{2}$$

We use the undeformed drop radius R and the inverse shear rate $\dot{\gamma}^{-1}$ as the length and the time scales, respectively, for nondimensionalizing the problem. Four nondimensional parameters define the system in its steady state: Reynolds number $\mathrm{Re} = \rho\dot{\gamma}R^2/\mu$, capillary number $Ca = (\dot{\gamma}\mu R)/\Gamma$, viscosity ratio $\lambda = \mu_d/\mu$ and density ratio $\lambda_\rho = \rho_d/\rho$. The subscript $_d$ represents the drop phase. We fix $\lambda_\rho = 1$ throughout the simulations.

B. Bulk stress and rheological functions for emulsion

The bulk stress for the emulsion in a simple shear can be taken as a volume average. Such averaged stress is equivalent to the stress measured in a homogeneous shear experiment (Batchelor 1970). Let V be the averaging volume, V_d and A_d be the volume and surface area of a typical drop. For both the drop and the ambient fluid being Newtonian, the averaged stress $\boldsymbol{\sigma}^{\mathrm{ave}}$ can be expressed as [Batchelor (1970); Mellema and Willemse (1983); Onuki (1987)]:

$$\boldsymbol{\sigma}^{\mathrm{ave}} = \frac{1}{V}\int_V (\boldsymbol{\sigma} - \rho\mathbf{u'u'})dV = -P_{\mathrm{ave}}\mathbf{I} + \boldsymbol{\tau}_{\mathrm{ave}} + \frac{\mu_d - \mu}{V}\sum\int_{A_d}(\mathbf{un} + \mathbf{nu})dA$$

$$-\frac{\Gamma}{V}\sum\int_{A_d}\left(\mathbf{nn} - \frac{\mathbf{I}}{3}\right)dA - \frac{1}{V}\int_V \rho\mathbf{u'u'}dV = -P_{\mathrm{ave}}\mathbf{I} + \boldsymbol{\tau}_{\mathrm{ave}} + \boldsymbol{\sigma}^{\mathrm{excess}}, \tag{3}$$

where P_{ave} is the isotropic part of the average "component" stress [Jansseune (2000)], $\mathbf{I}$ the identity tensor, and $\boldsymbol{\tau}_{\mathrm{ave}}$ is the deviatoric part of the average "component" stress. $\boldsymbol{\sigma}^{\mathrm{excess}}$ represents the contribution due to the presence of drops, giving rise to nonzero normal stress difference in a shear flow. The excess stress is composed of three parts:

$$\boldsymbol{\sigma}^{\mathrm{excess}} = \boldsymbol{\sigma}^{\mathrm{vis}} + \boldsymbol{\sigma}^{\mathrm{int}} + \boldsymbol{\sigma}^{\mathrm{ptb}}, \tag{4}$$

where

$$\boldsymbol{\sigma}^{\mathrm{vis}} = \frac{\mu_d - \mu}{V}\sum\int_{A_d}(\mathbf{un} + \mathbf{nu})dA, \quad \boldsymbol{\sigma}^{\mathrm{int}} = -\Gamma\mathbf{q}, \quad \boldsymbol{\sigma}^{\mathrm{ptb}} = -\frac{1}{V}\int_V \rho\mathbf{u'u'}dV. \tag{5}$$

$$\mathbf{q} = \frac{1}{V}\sum\int_{A_d}\left(\mathbf{nn} - \frac{\mathbf{I}}{3}\right)dA, \tag{6}$$

the anisotropy or interface tensor, is a geometric quantity. $\mathbf{n}$ is the outward unit normal vector at the drop interface. The sum is over all drops that are present in the averaging volume V. Note that fluid inertia affects fluid velocity and motion of the interface. The interfacial stress is proportional to the interface tensor $\mathbf{q}$, which is determined by the motion of the interface, and thereby indirectly by inertia. $\boldsymbol{\sigma}^{\mathrm{ptb}}$ is a stress arising from the perturbation velocity at finite inertia. $\mathbf{u'} = \mathbf{u} - \bar{\mathbf{u}}$ is the perturbation or fluctuation velocity, while $\bar{\mathbf{u}}$ is the unperturbed velocity. Note that $\boldsymbol{\sigma}^{\mathrm{ptb}}$ resembles Reynolds stress computed in turbulent flows. For system with $\lambda = 1$, the stress due to viscosity difference $\boldsymbol{\sigma}^{\mathrm{vis}}$ becomes zero.

Even though the formulation and the numerical simulation can treat a concentrated emulsion, here we consider only a dilute emulsion. The drops do not interact with each other and we can use the computation of the flow field due to a single drop in a shear. In this limit the contribution of each drop to the bulk stress is independent. For a dilute system of m identical droplets in V with volume V_d and surface area A_d, the interface tensor (6) varies linearly with the droplet volume fraction $\Phi = m V_d / V$:

$$\mathbf{q} = \Phi \mathbf{q}_d, \quad \mathbf{q}_d = \frac{1}{V_d} \int_{A_d} \left(\mathbf{nn} - \frac{\mathbf{I}}{3} \right) dA. \tag{7}$$

The interfacial stress nondimensionalized by $\mu \dot{\gamma}$ is expressed as

$$\mathbf{\Sigma}^{\text{int}} = \frac{\boldsymbol{\sigma}^{\text{int}}}{\mu \dot{\gamma}} = \Phi \mathbf{\Sigma}_d^{\text{int}}, \quad \mathbf{\Sigma}_d^{\text{int}} = -\frac{\Gamma}{\mu \dot{\gamma}} \mathbf{q}_d = -\frac{R}{Ca} \mathbf{q}_d. \tag{8}$$

For the nondimensional perturbation stress $\mathbf{\Sigma}^{\text{ptb}}$, a volume integral [see Eq. (5)], the superposition and the corresponding linearity with Φ holds at extreme dilution:

$$\mathbf{\Sigma}^{\text{ptb}} = \frac{\boldsymbol{\sigma}^{\text{ptb}}}{\mu \dot{\gamma}} = \Phi \mathbf{\Sigma}_d^{\text{ptb}}, \quad \mathbf{\Sigma}_d^{\text{ptb}} = -\frac{1}{m \mu \dot{\gamma} V_d} \int_V \rho \mathbf{u}' \mathbf{u}' dV = -\frac{\text{Re}}{m V_d} \int_V \frac{\mathbf{u}' \mathbf{u}'}{(\dot{\gamma} R)^2} dV. \tag{9}$$

The nondimensional excess stress for $\lambda = 1$ is given by

$$\mathbf{\Sigma}^{\text{excess}} = \Phi \mathbf{\Sigma}_d^{\text{excess}} = \mathbf{\Sigma}^{\text{int}} + \mathbf{\Sigma}^{\text{ptb}} = \Phi(\mathbf{\Sigma}_d^{\text{int}} + \mathbf{\Sigma}_d^{\text{ptb}}). \tag{10}$$

Because we restrict ourselves to a dilute emulsion, we calculate the single-drop stresses $\mathbf{\Sigma}_d^{\text{int}}, \mathbf{\Sigma}_d^{\text{ptb}}, \mathbf{\Sigma}_d^{\text{excess}}$ and omit the subscript "d" in the following.

The constitutive properties of any complex fluids in simple shear are completely determined by three rheological functions—effective viscosity μ_e, first normal stress difference N_1 and second normal stress difference N_2. According to above stress definitions, the rheological functions are expressed as:

$$\frac{\mu_e}{\mu} = 1 + \Sigma_{12}^{\text{excess}}, \tag{11}$$

$$N_1 = N_1^{\text{excess}} = \Sigma_{11}^{\text{excess}} - \Sigma_{22}^{\text{excess}}, \tag{12}$$

$$N_2 = N_2^{\text{excess}} = \Sigma_{22}^{\text{excess}} - \Sigma_{33}^{\text{excess}}. \tag{13}$$

Note that the interfacial stress is directly related to the morphology of drops. We define an orientation angle θ as the angle between axis of drop extension and the x axis coincidental with imposed velocity. Note that the axis of drop extension is the same as the principal axis of the $\mathbf{q}$ tensor with the largest eigenvalue. A relation between θ and interfacial rheological functions was reported by Jansseune *et al.* (2000):

$$\frac{N_1^{\text{int}}}{\Sigma_{12}^{\text{int}}} = 2 \cot(2\theta). \tag{14}$$

III. NUMERICAL METHODS

The incompressible flow satisfying Eq. (1) is solved by Front-tracking finite-difference method. The method treats the entire flow system as a single phase with material properties varying sharply in a thin region (four grid points) across the interface [Tryggvason *et al.* (2001)]. The interfacial tension is treated as a distributed force over the same region

by smearing out the Dirac δ-function in Eq. (1). A three-dimensional staggered grid is used for the entire domain and a surface triangular grid is used to discretize the drop surface (front). The single phase flow is then solved by an operator-splitting/projection finite-difference method. The velocity at the three-dimensional grid is interpolated to front nodes, and the front is updated to obtain its new position. An adaptive front regridding scheme is implemented to avoid excessive front-element distortion. The explicit scheme inherently suffers from severe diffusion-limited restrictions on time steps at low Reynolds numbers. To overcome it, we treat the diffusive terms semi-implicitly in alternate spatial directions (ADI). Detailed scheme are provided in Sarkar and Schowalter (2001a); Li and Sarkar (2005a). ADI enhances the efficiency of the simulation by one order of magnitude. The interfacial stress and the perturbation stress in Eq. (5) are computed by numerical integration over the drop surface and the computational domain, respectively.

IV. RESULTS

We study the dilute emulsion by simulating a single drop between two large plates separated by length L_{sp} in the y direction as in Fig. 1(a). Initially, a spherical drop with radius R is injected into the shear flow. We simulate the flow and deformation in a rectangular domain [Fig. 1(b)]. Periodic boundary conditions are specified in the x and z direction, and wall boundary conditions in the y direction. We use a box of size $L_x = 10R$, $L_y = L_{sp} = 10R$ and $L_z = 5R$ and a $96 \times 96 \times 48$ grid for most simulations. We checked the convergence of the simulation by increasing the discretization to $160 \times 160 \times 80$ without significant changes in the result. We also enlarged the simulation domain in all three directions and observed little change in drop deformation $D = (L - B)/(L + B)$ (L is the maximum axis and B the minimum axis) as shown in Fig. 2(a). The resulting interfacial stress N_1^{int} also shows little dependence on the size of the domain [Fig. 2(b)]. The perturbation stress N_1^{ptb}, however, varies drastically with the domain size [Fig. 2(c)]. Although the shape of the drop and the flow field in its neighborhood can be accurately captured by the simulation in the $10R \times 10R \times 5R$ domain, the volume-integrated perturbation stress [Eq. (5)] depends strongly on the system size. On the other hand, simulation in a larger domain with same level of discretization is prohibitively costly. We adopt a two-step procedure to compute the perturbation stress. The drop shape and the nearby flow are first obtained by a $10R \times 10R \times 5R$ box simulation. The velocity field at the surface of the central $5R \times 5R \times 2.5R$ sub-domain is used as an internal boundary to find the flow field in a much larger box using coarse grid calculation [inset of Fig. 2(d)]. The perturbation stress is then computed from the coarse-grid velocity field. The convergence of the coarse-grid perturbation stress computation is shown in Fig. 2(d). The $60R \times 60R \times 60R$ domain is used for all calculations. The two-step calculation provides an efficient way for predicting the perturbation stress.

In the following sections, we first present the results on drop morphology and then focus on the rheology. Simulations at low Reynolds number (Re=0.1) are compared with analytical theories and available experimental data in Stokes flow. The comparison validates present simulation as a tool to study emulsion rheology. The deviation at higher Reynolds number indicates significant contribution of inertia. Capillary number and Reynolds number are systematically varied in the investigation.

A. Drop morphology

In Fig. 3, we compare the transient drop axes versus flow strain $\gamma = \dot{\gamma} t$ with experimental data of small deformation (a) (Guido and Villone 1998) and large deformation (b)
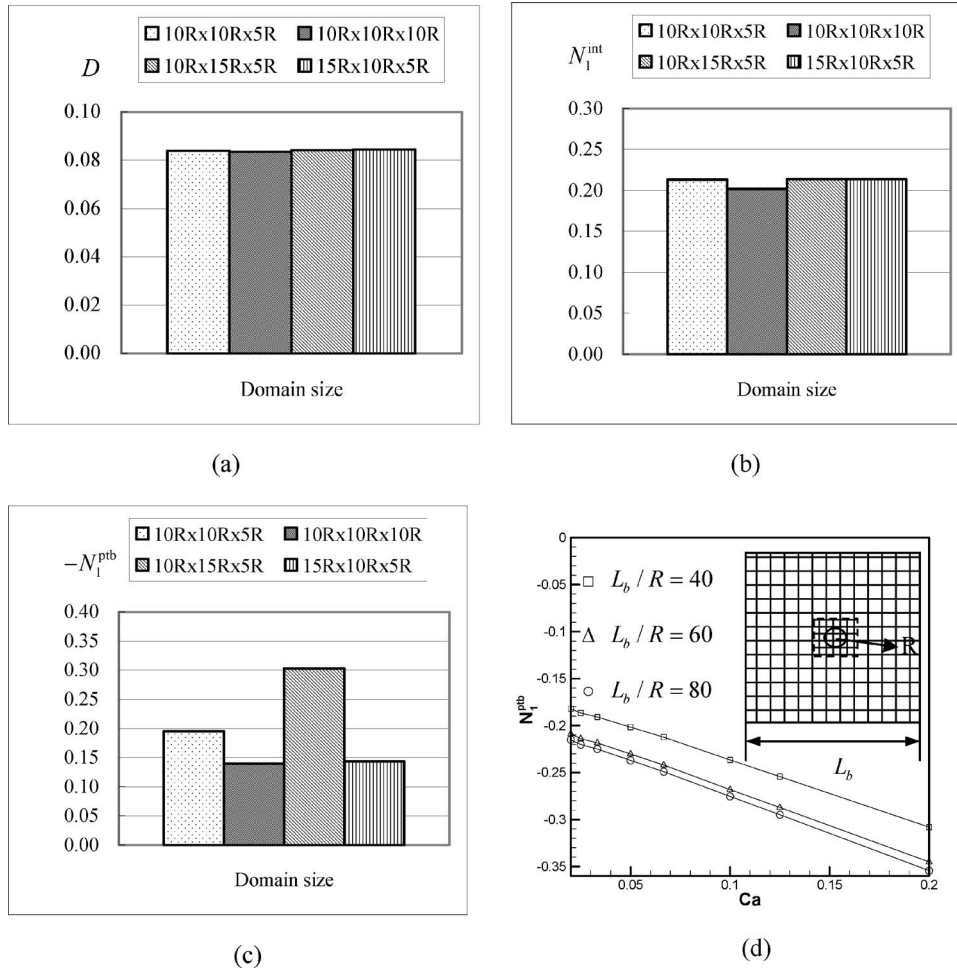
FIG. 2. Convergence of deformation D (a) and interfacial stress N_1^{int} (b) with varying sizes of simulation domain for Re=1.0 Ca=0.0667. (c) Shows the divergence of the corresponding perturbation stress $-N_1^{ptb}$. The convergence of $-N_1^{ptb}$ using coarse-grid computation for Re=1.0 is shown in (d).

and (c) [Almusallam *et al.* (2000)]. In Fig. 3(a), the simulation for Re=0.1 is shown to compare well with experimental measurements. The same set of data is matched by the prediction of ellipsoidal tensor models [from Fig. 2 in Yu and Bousmina (2003)]. We show the results for Re=1.0 in the same plot. Increased inertia leads to larger deformation indicated by larger L and smaller B and W (the axis in z direction) in the final steady state. In Fig. 3(b), our simulation at Re=0.1 matches the experimental data of W but slightly overpredicts L and underpredicts B. The drop eventually breaks up at such supercritical conditions. Increasing Re to 1.0 does not significantly modify the drop axes. The large capillary number (Ca=5.0) implies small interfacial forces compared to the viscous force. Under this condition, the flow configuration becomes independent of Re. The Reynolds-number independence of axes evolution is more prominent in Fig. 3(c) with an even larger Ca (Ca=70.0). The W axis remains constant under this condition.

In Fig. 4, we compare the deformation parameter D=$(L-B)/(L+B)$ and orientation angle θ in steady state with the experiments by Torza *et al.* (1972). The simulations of
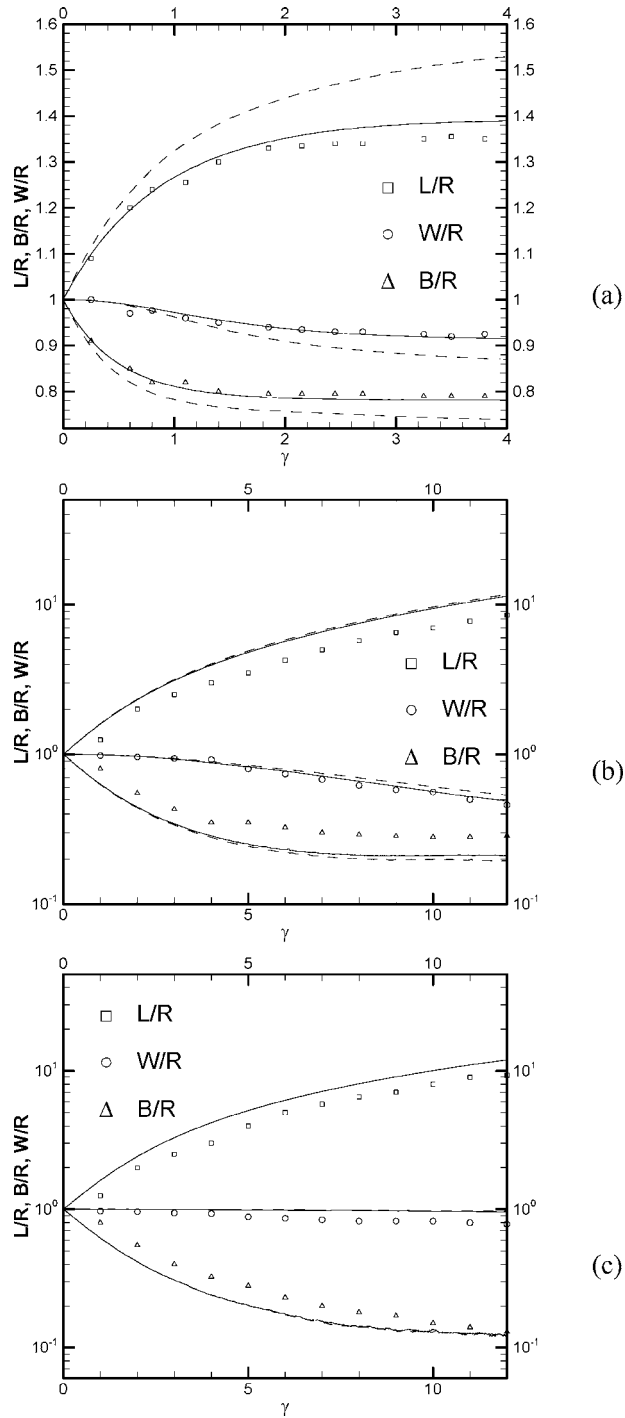
FIG. 3. Transient evolution of drop axis. (a) $\lambda = 1.4$, $Ca = 0.24$ (b) $\lambda = 1.0$, $Ca = 5.0$ and (c) $\lambda = 1.0$, $Ca = 70.0$; Symbols are experimental data from Guido and Villone (1998) in (a) and Almusallam *et al.* (2000) in (b) and (c); For (a)–(c), —— Re = 0.1, ------ Re = 1.0.
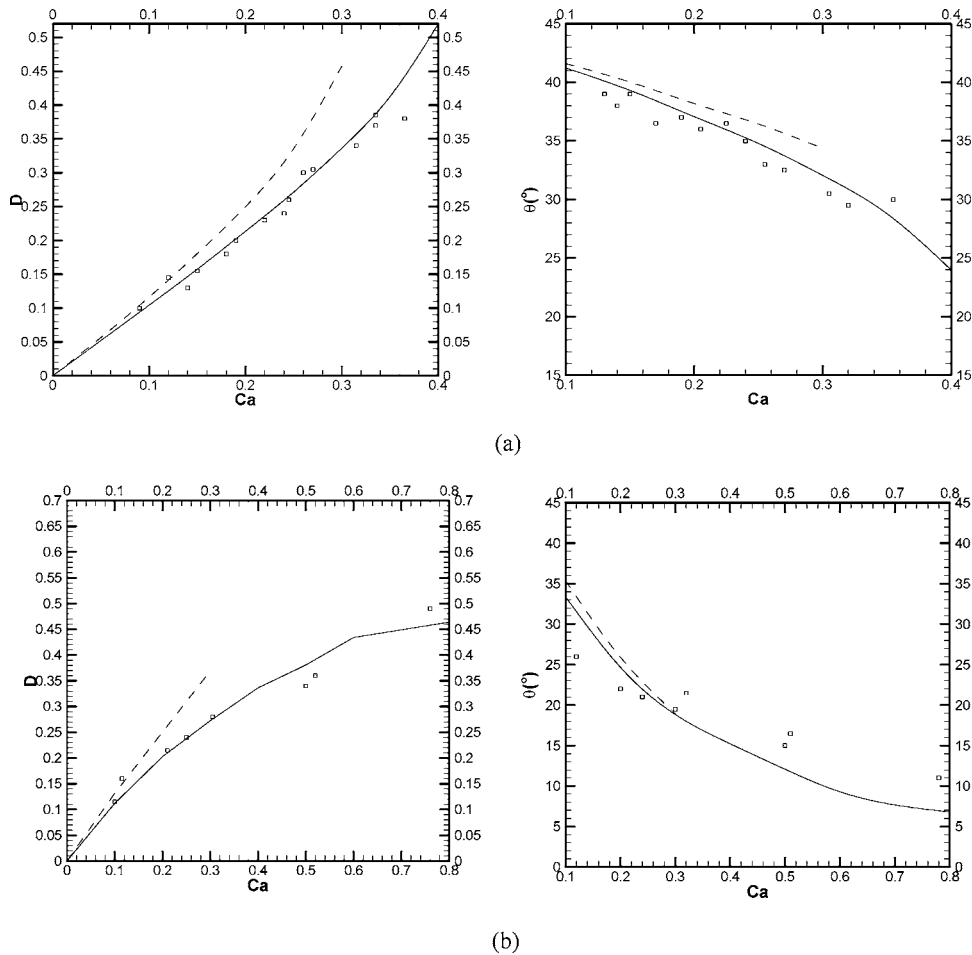
(a)

(b)

FIG. 4. Steady state deformation D and orientation angle θ vs Ca; (a) $\lambda=0.08$ (b) $\lambda=3.6$. Symbols represent experimental data from Torza *et al.* (1972); For both (a) and (b), — Re=0.1, ------ Re=1.0.

both D and θ at Re=0.1 for different Ca match well with the experimental data. D increases and θ decreases with Ca for both low [$\lambda=0.08$ Fig. 4(a)] and high [$\lambda=3.6$ Fig. 4(b)] viscosity ratios. Increased inertia (Re=1.0) leads to larger D and θ at large Ca [in contrast to Fig. 3(c) for the same viscosity inside and outside the drop]. The changes in deformation and tilt angle due to inertia have important effects on the system rheology, as we will see next.

B. Shear rheology in low Reynolds number limit

In Fig. 5, we plot the steady-state interfacial stresses versus Ca at Re=0.1, and compare with small deformation theory of Choi and Schowalter (1975) (CS model) and tensor model by Yu *et al.* (2002) and Grmela *et al.* (2001) (referred to as GBP model) (See Appendixes A and B for detailed expressions). For brevity, we consider only $\lambda=1$. The CS model of small deformation predicts the shear stress Σ_{12}^{int} to be independent of Ca [Fig. 5(a)], i.e., the effective viscosity μ_e^{int} is constant [see Eq. (11)]. Similar trends are predicted by the GBP model at small Ca (small deformation limit). But for larger Ca, both GBP model and our simulation predict a shear thinning behavior, i.e., decreasing Σ_{12}^{int}
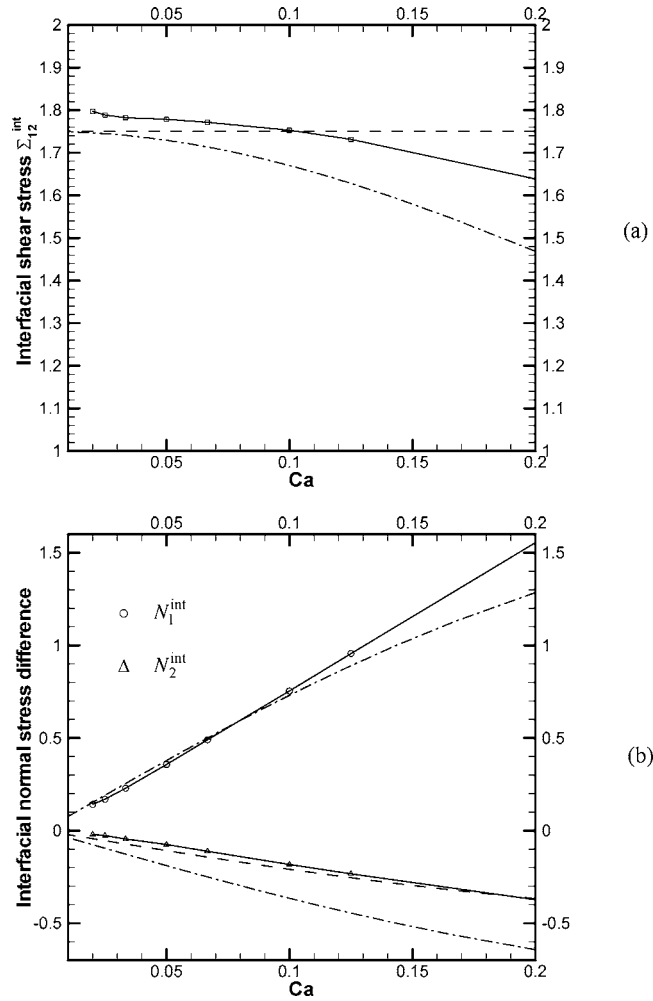
FIG. 5. (a) Interfacial shear stress and (b) normal stress differences vs *Ca*. The simulation results at Re=0.1 (line with symbols) are compared with CS model (----) and GBP-YB model (-·--·--).

with increasing *Ca*. In Fig. 5(b), our simulation predicts an increasing positive N_1^{int} and decreasing negative N_2^{int} with increasing *Ca*. As $Ca \rightarrow 0$, N_1^{int} and N_2^{int} asymptotically approach zero, the limiting value at zero shear rate [see also Eqs. (A6) and (A7)]. Our simulation compares well with CS and GBP models for most *Ca* considered. The results for N_1^{int} are better matched at small capillary numbers. For N_2^{int}, prediction of the CS model agrees with our simulation. $\mathbf{\Sigma}^{int}$ is determined by the interface tensor $\mathbf{q}$, which is affected by both deformation and orientation of the drop. The drop tends to be more deformed and at the same time better aligned with the flow at higher *Ca*. The combined effects give rise to an increased N_1^{int} and decreased N_2^{int} and Σ_{12}^{int}.

C. Effects of inertia on interfacial stresses

As Reynolds number increases, inertial force starts to play a role in determining the equilibrium drop morphology and velocity field. In Fig. 6, we plot the steady-state interfacial stresses versus *Ca* at Re=1.0 (solid) and compare it with Re=0.1 (dashed). The
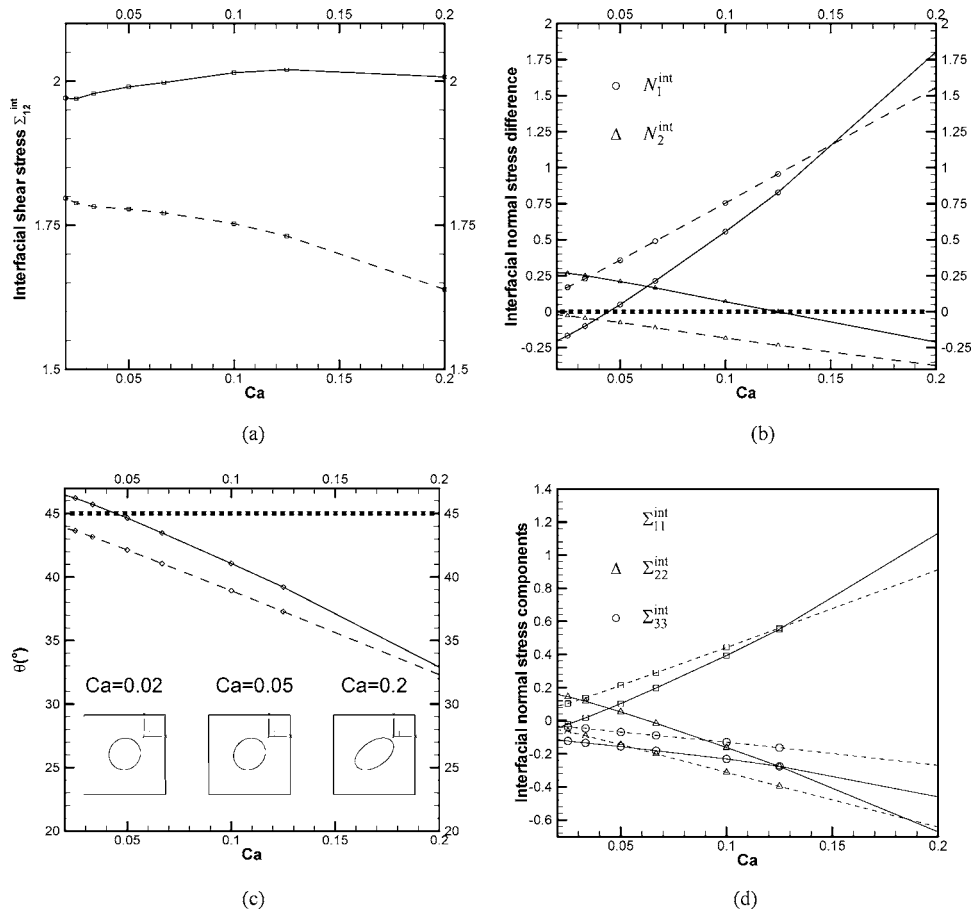
FIG. 6. (a) Interfacial shear stress vs Ca, (b) Interfacial normal stress difference vs Ca. (c) Steady state orientation angle θ vs Ca. Inset shows the drop shape in the x-y plane cut through the drop center at Re=1.0. (d) Interfacial normal stresses vs Ca. For (a)–(d), ------- Re=0.1, —— Re=1.0.

shear stress Σ_{12}^{int} at Re=1.0 is larger than that at Re=0.1 for all values of Ca [Fig. 6(a)]. It results from an increased q_{12} due to enhanced deformation and increased orientation angle at higher inertia (Fig. 4). Note that further increase of Re leads to drop breakup at Ca=0.2. We did not investigate the stress beyond drop breakup. With increasing Ca, Σ_{12}^{int} first increases and then decreases above Ca=0.13, i.e. slight shear thickening followed by shear thinning. It is a result of the competition between enhanced deformation and decreased orientation angle with increasing Ca. In Fig. 6(b), we observe that the first normal stress difference N_1^{int} increases with increasing Ca for Re=1.0 at a faster rate than Re=0.1. Below $Ca \approx 0.045$, N_1^{int} for Re=1.0 is negative and it changes to positive values above $Ca \approx 0.045$. Similar transition from positive to negative values is observed for N_2^{int} at $Ca \approx 0.12$. In contrast to Stokes flow, N_1^{int} and N_2^{int} approaches nonzero values as Ca vanishes at finite inertia. The change of sign for N_1^{int} and N_2^{int} is related to drop orientation. In Fig. 6(c), the steady-state orientation angle θ versus Ca is plotted for both Re=0.1 and Re=1.0. θ decreases with increasing Ca but remains smaller than $\pi/4$ for all value of Ca at Re=1.0. At Re=1.0, θ is more than $\pi/4$ for small Ca till $Ca \approx 0.045$, as was also observed by Renardy and Cristini (2001). In the inset, the change of orientation is illus-

trated by the drop shape in the x-y plane through the center of the drop. The interfacial stresses are directly related to the orientation angle θ [Eq. (14)]. In fact, $\theta = \pi/4$ corresponds to $q_{11} = q_{22}$ and is the point for sign change of N_1^{int}. To better understand the sign change in N_2^{int}, we plot in Fig. 6(d) the actual components of the normal stress for the two Reynolds numbers. Σ_{11}^{int} matches with Σ_{22}^{int} at $Ca \approx 0.045$ and Σ_{22}^{int} with Σ_{33}^{int} at $Ca \approx 0.12$ (corresponding to the sign changes in N_1^{int} and N_2^{int}). Note that Σ_{33}^{int} in the vorticity direction experiences only a parallel shift while Re=0.1 is changed to Re=1.0, in contrast to the change in the rates of increase in Σ_{11}^{int} and decrease in Σ_{22}^{int} with Ca, the latter being stress components in the plane of the flow. The change in orientation angle θ in the flow plane at higher inertia causes the flow-plane normal stresses to change their behaviors. Σ_{33}^{int} behavior possibly is governed by the constraint $\Sigma_{11}^{\text{int}} + \Sigma_{22}^{\text{int}} + \Sigma_{33}^{\text{int}} = 0$, and results in the change in sign of N_2^{int}.

Figure 7 shows the Reynolds number dependence of interfacial stresses at $Ca = 0.05$ (solid) and $Ca = 0.02$ (dashed). In Fig. 7(a) the shear stress Σ_{12}^{int} increases with increasing Re. As Ca is increased from 0.02 to 0.05, Σ_{12}^{int} increases (shear thickening) at large Re. In Fig. 7(b), the first normal stress difference N_1^{int} decreases from positive to negative values as Re increases while the second normal stress difference N_2^{int} shows an opposite trend. The critical Re value for the sign change of N_1^{int} is smaller for smaller Ca. ($\text{Re}_c \approx 0.4$ for $Ca = 0.02$ and $\text{Re}_c \approx 1.2$ for $Ca = 0.05$). Figure 7(c) shows the steady-state θ versus Re. θ increases and reaches values beyond $\pi/4$ with increasing Re. The critical Re for the sign change of N_1^{int} [Fig. 7(b)] corresponds to $\theta = \pi/4$ [Fig. 7(c)].

D. Perturbation stresses

Finite inertia and interfacial tension lead to a flow perturbation and an effective stress [Eq. (5)] in addition to the interfacial stress. The perturbation stress is calculated using the coarse grid simulation as mentioned before. In Fig. 8(a), the perturbation stresses are plotted as a function of Ca for Re=1.0. Σ_{12}^{ptb} is positive and increases slightly with increasing Ca. Compared to $\Sigma_{12}^{\text{int}}(\approx 2.0)$, $\Sigma_{12}^{\text{ptb}}(\approx 0.05)$ is negligible. N_1^{ptb} and N_2^{ptb} are both negative and the former is larger in magnitude. With increasing Ca, N_1^{ptb} decrease while N_2^{ptb} increases. In Fig. 8(b), perturbation stresses are plotted as a function of Re for $Ca = 0.05$. As Re→0, all perturbation stresses vanish. N_1^{ptb} decreases with increasing Re while Σ_{12}^{ptb} increases with Re. N_2^{ptb} is negative at relatively small Re (Re<2.0) and changes sign from negative to positive as Re increases.

E. Total excess stresses

Figure 9 summarizes the steady-state excess stresses Σ^{excess} ($\Sigma^{\text{int}} + \Sigma^{\text{ptb}}$) as functions of Ca [Fig. 9(a)] and Re [Fig. 9(b)]. $\Sigma_{12}^{\text{excess}}$ increases with Ca for Re=1.0 but decreases with Ca for Re=0.5 and Re=0.1. This behavior is similar to that of just the interfacial part Σ_{12}^{int} [Fig. 6(a)], interfacial part of the excess stress dominates the part due to perturbation. N_1^{excess} and N_2^{excess} change signs as Ca varies for Re=0.5 and Re=1.0. Once again the same trends are observed for N_1^{int} and N_2^{int} [Fig. 6(b)]. The sign change of N_1^{excess} has important physical significance. At small Reynolds number (Re=0.1), positive $N_1^{\text{excess}} = \Sigma_{11}^{\text{excess}} - \Sigma_{22}^{\text{excess}}$ indicates that a compressive force acts in the media bringing the plates together. However, finite inertia leads to negative N_1^{excess}, i.e., a tensile force acts pushing the plates away from each other. In Fig. 9(b), $\Sigma_{12}^{\text{excess}}$ increases with increasing Re for both $Ca = 0.02$ and $Ca = 0.05$. $N_1^{\text{excess}}(N_2^{\text{excess}})$ is positive (negative) at small Re and decreases (increases) with Re. Both of them change sign as Re is increased. Note the similarity with Fig. 7 for just the interfacial part. Note that for a suspension of rigid particles, two-dimensional computation of Patankar and Hu (2002) indicated shear thickening and a
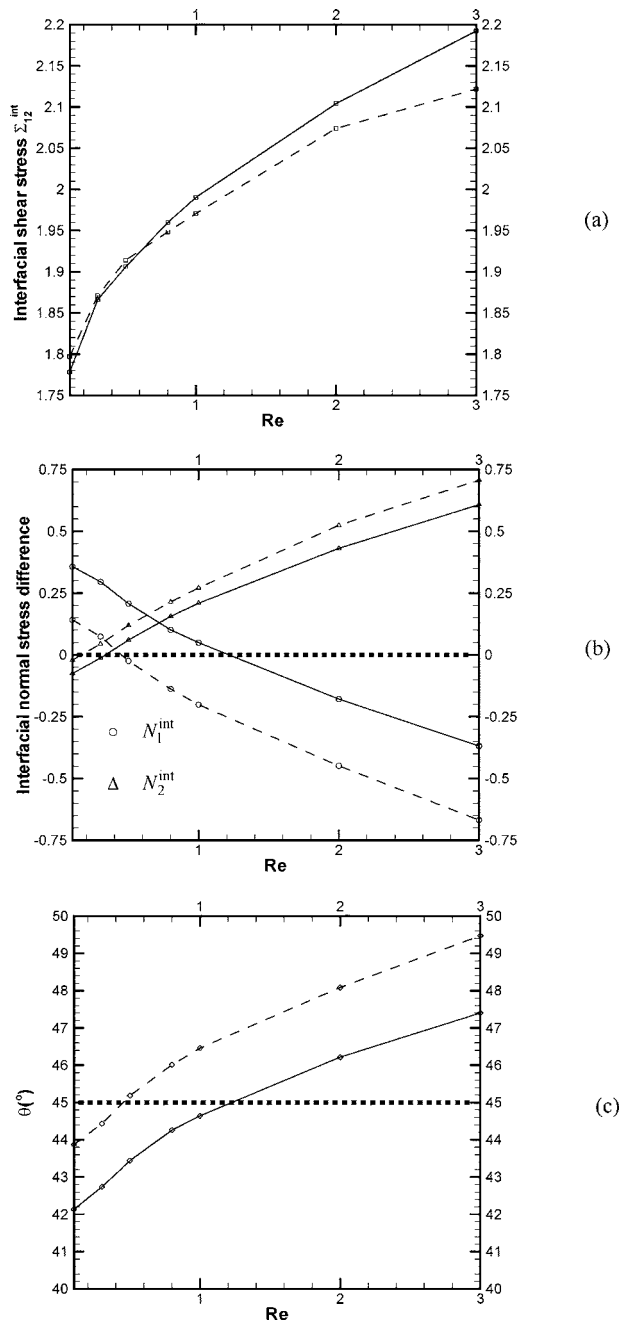
FIG. 7. (a) Interfacial shear stress and (b) first normal stress difference vs Re. (c) Steady state orientation angle θ vs Re. For (a)–(c), — $Ca=0.05$, ------ $Ca=0.02$.

negative first normal stress difference at finite inertia, which contrast with the present result due to the drop deformability and the finite interfacial tension. Recently, in steady shear negative normal stresses were measured for attractive emulsion by Montesi *et al.* (2004) and for suspension of non-Brownian multi-walled carbon nanotubes by Lin-
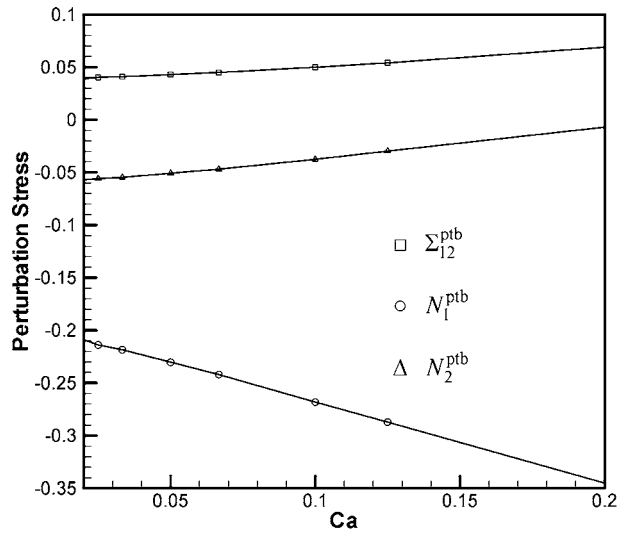
(a)
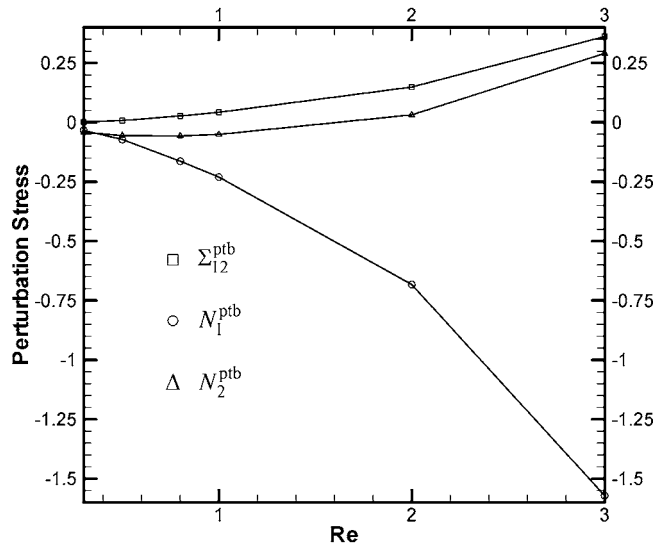
(b)

FIG. 8. (a) Perturbation stresses vs *Ca* at Re=1.0. (b) Perturbation stresses vs Re at *Ca*=0.05.

Gibson *et al.* (2004). In both cases interaction between elements (drops or nanotubes) play critical role and form cylindrical aggregates aligned along the vorticity direction.

V. CONCLUDING REMARKS

We performed a numerical investigation of the rheology of dilute emulsion in shear flow at finite inertia. We used front-tracking finite-difference method to simulate the flow
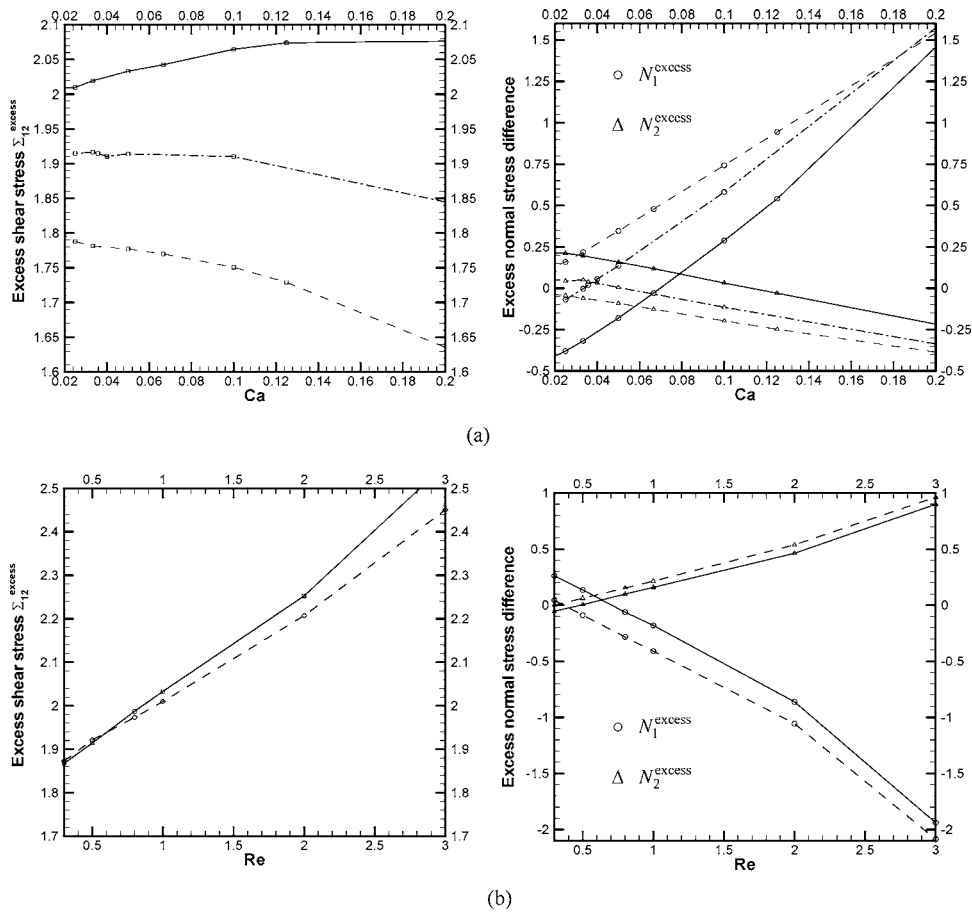
FIG. 9. (a) Total excess stresses vs Ca at Re=1.0 (—), Re=0.5 (–·–·) and Re=0.1 (------). (b) Total excess stresses vs Re at Ca=0.05 (—) and Ca=0.02 (------).

as well as exact drop shape. The results of simulation agree with experimental data and predictions of analytical models at vanishing Reynolds number. The excess stress due to presence of drops consists of two parts—one due to interfacial tension at the drop boundary and the other due to the flow perturbation due to the drop, the later being present only at finite inertia. The first part is normally much larger in magnitude. With increased Reynolds number, the emulsion changes from shear thinning to shear thickening due to the competition between enhanced deformation and decreased orientation angle. In contrast to the Stokes flow case, the first normal stress difference becomes negative at small capillary number or large Reynolds number due to a drop tilt angle greater than forty-five degree. On the other hand, the second normal stress, which is negative for Stokes flow, becomes positive at small capillary numbers or large Reynolds numbers. A compressive force is required to maintain plate separation due to the negative first normal stress difference occurring at finite inertia.

ACKNOWLEGMENTS

APPENDIX: ANALYTICAL MODELS FOR EMULSION RHEOLOGY

1. Choi-Schowalter model

Choi and Schowalter (1975) developed a rheological model for emulsion in steady shear Stokes flow based on the small deformation perturbation analysis. As the volume fraction $\Phi \rightarrow 0$, the rheological functions vary linearly with volume fraction Φ. Consider the viscosity ratio $\lambda = 1$, the interfacial rheological functions are reduced to:

$$\Sigma_{12}^{CS} = \frac{\mu_e^{CS}}{\mu} = \frac{5\lambda + 2}{2(\lambda + 1)}\Phi \overset{\lambda=1}{=} \frac{7}{4}\Phi, \tag{A1}$$

$$N_1^{CS} = \frac{2}{5}\frac{19\lambda + 16}{4(\lambda + 1)}\frac{Ca}{1 + Z^2}\Phi \overset{\lambda=1}{=} \frac{245}{32}\frac{Ca}{(1 + Z^2)}\Phi, \tag{A2}$$

$$N_2^{CS} = -\frac{1}{280}\frac{(19\lambda + 16)(29\lambda^2 + 61\lambda + 50)}{4(\lambda + 1)^3}\frac{Ca}{1 + Z^2}\Phi \overset{\lambda=1}{=} -\frac{35}{16}\frac{Ca}{(1 + Z^2)}\Phi, \tag{A3}$$

where

$$Z = \frac{(19\lambda + 16)(2\lambda + 3)}{40(\lambda + 1)}Ca \overset{\lambda=1}{=} \frac{35}{16}Ca. \tag{A4}$$

2. Grmela-Bousmina-Palierne model

Based on Grmela, Bousmina, and Palierne's (2001) morphological tensor model, Yu *et al.* (2002) calculated the interfacial rheological functions for emulsion in shear Stokes flow. Shear-rate dependence of viscosity is taken into account. The expressions for these functions as $\Phi \rightarrow 0$ are:

$$\Sigma_{12}^{GBP} = \frac{\mu_e^{GBP}}{\mu} = \frac{4(2\lambda + 3)}{25}\frac{f_1 f_2^2}{(Ca^2 + f_1^2)}\Phi = \frac{4(2\lambda + 3)}{25}\frac{f_2^2}{f_1(Z^2 + 1)}\Phi \overset{\lambda=1}{=} \frac{7}{4}\frac{1}{(Z^2 + 1)}\Phi, \tag{A5}$$

$$N_1^{GBP} = \frac{8(2\lambda + 3)}{25}\frac{Ca f_2^2}{(Ca^2 + f_1^2)}\Phi = \frac{8(2\lambda + 3)}{25}\frac{Ca f_2^2}{f_1^2(Z^2 + 1)}\Phi \overset{\lambda=1}{=} \frac{245}{32}\frac{Ca}{(Z^2 + 1)}\Phi, \tag{A6}$$

$$N_2^{GBP} = -\frac{1}{2}N_1^{GBP} \overset{\lambda=1}{=} -\frac{245}{64}\frac{Ca}{(Z^2 + 1)}\Phi, \tag{A7}$$

where

$$f_1 = \frac{40(\lambda + 1)}{(2\lambda + 3)(19\lambda + 16)} = \frac{Ca}{Z} \overset{\lambda=1}{=} \frac{16}{35}, \tag{A8}$$

$$f_2 = \frac{5}{2\lambda + 3} \overset{\lambda=1}{=} 1. \tag{A9}$$

Note that $N_1^{GBP} = N_1^{CS}$, $N_2^{GBP} = \frac{7}{4}N_2^{CS}$ and $\Sigma_{12}^{GBP} \rightarrow \Sigma_{12}^{CS}$ as $Ca \rightarrow \infty$.

References

Almusallam, A. S., R. G. Larson, and M. J. Solomon, "A constitutive model for the prediction of ellipsoidal droplet shapes and stresses in immiscible blends," J. Rheol. **44**, 1055–1083 (2000).

Aschoff, D., and P. Schümmer, "Evaluation of unsteady Couette-flow measurement under the influence of fluid inertia," J. Rheol. **37**, 1237–1251 (1993).

Batchelor, G. K., "The stress system in a suspension of force-free particles," J. Fluid Mech. **41**(3), 545–570 (1970).

Böhme, G., and M. Stenger, "On the influence of fluid inertia in oscillatory rheometry," J. Rheol. **34**, 415–424 (1990).

Choi, S. J., and W. R. Schowalter, "Rheological properties of nondilute suspensions of deformable particles," Phys. Fluids **18**, 420–427 (1975).

Cristini, V., R. W. Hooper, C. W. Macosko, M. Simeone, and S. Guido, "A numerical and experimental investigation of lamella blend morphologies," Ind. Eng. Chem. Res. **41**, 6305–6311 (2002a).

Cristini, V., C. W. Macosko, and T. Jansseune, "A note on transient stress calculation via numerical simulations," J. Non-Newtonian Fluid Mech. **105**, 177–187 (2002b).

Cristini, V., S. Guido, A. Alfani, J. Blawzdziewicz, and M. Loewenberg, "Drop breakup and fragment size distribution in shear flow," J. Rheol. **47**, 1283–1298 (2003).

Doi, M., and T. Ohta, "Dynamics and rheology of complex interfaces. I," J. Chem. Phys. **95**, 1242–1248 (1991).

Grmela, M., M. Bousmina, and J. Palierne, "On the rheology of immiscible blends," Rheol. Acta **40**, 560–569 (2001).

Guido, S., and M. Villone, "Three-dimensional shape of a drop under simple shear flow," J. Rheol. **42**(2), 395–415 (1998).

Jackson, N. E., and C. L. Tucker III, "A model for large deformation of an ellipsoidal droplet with interfacial tension," J. Rheol. **47**(3), 659–682 (2003).

Jansseune, T., J. Mewis, P. Moldenaers, M. Minale, and P. L. Maffettone, "Rheology and rheological morphology determination in immiscible two-phase polymer model blends," J. Non-Newtonian Fluid Mech. **93**, 153–165 (2000).

Jansseune, T., I. Vinckier, P. Moldenaers, and J. Mewis, "Transient stresses in immiscible model polymer blends during start-up flows," J. Non-Newtonian Fluid Mech. **99**, 167–181 (2001).

Li, J., Y. Y. Renardy, and M. Renardy, "Numerical simulation of breakup of a viscous drop in simple shear flow through volume-of-fluid method," Phys. Fluids **12**(2), 269–282 (2000).

Li, X., and K. Sarkar, "Drop dynamics in an oscillating extensional flow at finite Reynolds numbers," Phys. Fluids **17**, 027103 (2005a).

Li, X., and K. Sarkar, "Numerical investigation of the rheology of a dilute emulsion of drops in an oscillating extensional flow," J. Non-Newtonian Fluid Mech. (2005b, in press.

Lin, C., J. H. Peery, and W. R. Schowalter, "Simple shear flow round a rigid sphere: inertial effects and suspension rheology," J. Fluid Mech. **44**, 1–17 (1970).

Lin-Gibson, S., J. A. Pathak, E. A. Grulke, H. Wang, and E. K. Hobbie, "Elastic flow instability in nanotube suspensions," Phys. Rev. Lett. **92**(4), 048302 (2004).

Maffettone, P. L., and F. Greco, "Ellipsoidal drop model for single drop dynamics with non-Newtonian fluids," J. Rheol. **48**(1), 83–100 (2004).

Maffettone, P. L., and M. Minale, "Equations of change for ellipsoidal drops in viscous flow," J. Non-Newtonian Fluid Mech. **78**, 227–241 (1998).

Mellema, J., and M. W. M. Willemse, "Effective viscosity of dispersions approached by a statistical continuum method," Physica A **122**, 286–312 (1983).

Minale, M., "Deformation of a non-Newtonian ellipsoidal drop in a non-Newtonian matrix: extension of Maffetone-Manale model," J. Non-Newtonian Fluid Mech. **123**, 151–160 (2004).

Montesi, A., A. P. Alejandro, and M. Pasquali, "Vorticity alignment and negative normal stresses in sheared attractive emulsions," Phys. Rev. Lett. **92**(5), 058303 (2004).

Onuki, A., "Viscosity enhancement by domains in phase-separating fluids near the critical points: Proposal of critical rheology," Phys. Rev. A **35**(12), 5149–5155 (1987).

Patankar, N. A. and H. H. Hu, "Finite Reynolds number effect on the rheology of a dilute suspension of neutrally buoyant circular particles in a Newtonian fluid," Int. J. Multiphase Flow **28**, 409–425 (2002).

Renardy, Y. Y., and V. Cristini, "Effect of inertia on drop breakup under shear," Phys. Fluids **13**, 7–13 (2001).

Sarkar, K., and W. R. Schowalter, "Deformation of a two-dimensional drop at non-zero Reynolds number in time-periodic extensional flows: numerical simulation," J. Fluid Mech. **436**, 177–206 (2001a).

Sarkar, K., and W. R. Schowalter, "Deformation of a two-dimensional viscous drop in time-periodic extensional flows: analytical treatment," J. Fluid Mech. **436**, 207–230 (2001b).

Sarkar, K., and W. R. Schowalter, "Deformation of a two-dimensional viscoelastic drop at non-zero Reynolds number in time-periodic extensional flows," J. Non-Newtonian Fluid Mech. **95**, 315–342 (2000).

Taylor, G. I., "The viscosity of a fluid containing small drops of another fluid," Proc. R. Soc. London, Ser. A **138**, 41–48 (1932).

Taylor, G. I., "The formation of emulsions in definable fields of flow," Proc. R. Soc. London, Ser. A **146**, 501–523 (1934).

Torza, S., R. G. Cox, and S. G. Mason, "Particle motions in sheared suspensions XXVII. Transient and steady deformation and burst of liquid drops," J. Colloid Interface Sci. **38**, 395–411 (1972).

Tryggvason, G., B. Bunner, A. Esmaeeli, D. Juric, N. Al-Rawahi, W. Taubar, J. Han, S. Nas, and Y. J. Jan, "A front-tracking method for the computations of multiphase flow," J. Comput. Phys. **169**, 708–759 (2001).

Tucker, C. L., and P. Moldenaers, "Microstructural evolution in polymer blends," Annu. Rev. Fluid Mech. **34**, 177–210 (2002).

Velankar, S., P. V. Puyvelde, J. Mewis, and P. Moldenaers, "Effect of compatibilization on the breakup of polymeric drops in shear flow," J. Rheol. **45**(4), 1007–1019 (2001).

Velankar, S., P. V. Puyvelde, J. Mewis, and P. Moldenaers, "Steady-shear rheological properties of model compatibilized blends," J. Rheol. **48**(4), 725–744 (2004).

Wetzel, E. D., and C. L. Tucker, "Droplet deformation in dispersions with unequal viscosities and zero interfacial tension," J. Fluid Mech. **426**, 199–228 (2001).

Wylie, J. J., D. L. Koch, and A. J. C. Ladd, "Rheology of suspensions with high particle inertia and moderate fluid inertia," J. Fluid Mech. **480**, 95–118 (2003).

Yu, W., and M. Bousmina, "Ellipsoidal model for droplet deformation in emulsions," J. Rheol. **47**(4), 1011–1039 (2003).

Yu, W., M. Bousmina, M. Grmela, J. Palierne, and C. Zhou, "Quantitative relationship between rheology and morphology in emulsions," J. Rheol. **46**(6), 1381–1399 (2002).

Yu, W., M. Bousmina, C. Zhou, and C. L. Tucker, "Theory for drop deformation in viscoelastic systems," J. Rheol. **48**(2), 417–438 (2004).